Focal Plane Irradiance Statistics for Laser Downlink Beams

Saathof, Rudolf; Zadeh, Iman Esmaeil

DOI
10.1117/12.3069432

Publication date
2025

Document Version
Final published version

Published in
Environmental Effects on Light Propagation and Adaptive Systems VIII

Focal Plane Irradiance Statistics for Laser Downlink Beams

Rudolf Saathof[a] and Iman Esmaeil Zadeh[b]

[a]Delft university of Technology, Faculty of Aerospace Engineering, Department of Space Engineering, Kluyverweg 1 2628 HS, Delft, the Netherlands
[b]Delft university of Technology, Faculty of Applied Physics, Department of Imaging Physics, Lorentzweg 1 2628 CK Delft, the Netherlands

ABSTRACT

Laser satellite communications is a growing market for telecommunications services and secure communications. Due to the small footprint of the beam, it provides security, and it can serve as inherently safe communication, using the quantum properties of light, i.e. quantum communications, and quantum key distribution. For quantum communications, the detector sensitivity is of utmost importance. Hence, detector technologies such as Superconducting Nanowire Single Photon Detector (SNSPD), are designated to support optical communications. In this research, we estimate the efficacy of SNSPD arrays for optical downlinks to earth. In this paper, we investigate how spatial resolution of the SNSPD and the spatiotemporal statistics of the incoming turbulence can be matched, in order to effectively use SNSPD arrays. We simulated the downlink using a split-step approach, using a receiver aperture of 1 m and a Fried parameter of 50 and 12.5 cm (D/r_0 is 2 and 8). We obtained the average intensity, the scintillation index, the probability density function (PDF) and the power spectral density (PSD) using 4000 samples. We project instantaneous images on the SNSPD, to estimate how the PSD is distributed. We conclude that stronger turbulence conditions could improve detection performance, because the point spread function (PSD) is wider, and the incident light is distributed over more pixels.

Keywords: Laser satellite communications, Quantum Communications, Superconducting Nanowire Single Photon Detector, Optical Propagation trough Turbulence.

1. INTRODUCTION

Laser satellite communications is a growing market for telecommunications services and secure communications.[1] It is used complementary to radio frequency (RF) communications, to improve throughput, and alleviate the RF spectral bands. In addition, it provides security, due to the small footprint of the beam. Due to the optical carrier, it can serve as inherently safe communication, using the quantum properties of light, i.e. quantum communications, and quantum key distribution.[2] For quantum communications, the detector sensitivity is of utmost importance. Hence, detector technologies such as Superconducting Nanowire Single Photon Detector (SNSPD), are designated to support optical communications.

In this research, we estimate the efficacy of SNSPD arrays for optical downlinks to earth. We realize that the recovery time and spatial resolution of the SNSPD and the spatiotemporal statistics of the incoming turbulence need to be matched, in order to effectively use SNSPD arrays. In literature so far, some quantiative analysis is well known, such as the average point spread function, aperture averaged scintillation index, its probability density and time constants.[3,4] For example, the width of the average point spread function is related to the seeing conditions, which can be expressed by the Fried parater r_0, which is a measure of the coherence length of the phase disturbances. More detailed analysis of the statistics towards this direction are harder to find,[5,6] and are less straighforward to interpret. For the applications of SNSPDs in laser satellite links, we are interested in the spatiotemporal distributions in the focal plane, i.e. the average point spread function $\overline{I}(x,y) = \langle I(x,y,t)\rangle$, the scintillation index $\overline{\sigma_I^2}(x,y) = \langle \sigma_I^2(x,y,t)\rangle$, the probability density function ($p_{x,y}(I)$) and the power sprectral density ($S_{II}(x,y)$) all as a function of the focal plan coordinates.

Further author information: (Send correspondence to Rudolf Saathof)
Rudolf Saathof: E-mail: R.Saathof@Tudelft.NL

Environmental Effects on Light Propagation and Adaptive Systems VIII, edited by Karin Stein, Szymon Gladysz, Proc. of SPIE Vol. 13669, 136690M · 2025 Published by SPIE
0277-786X · doi: 10.1117/12.3069432

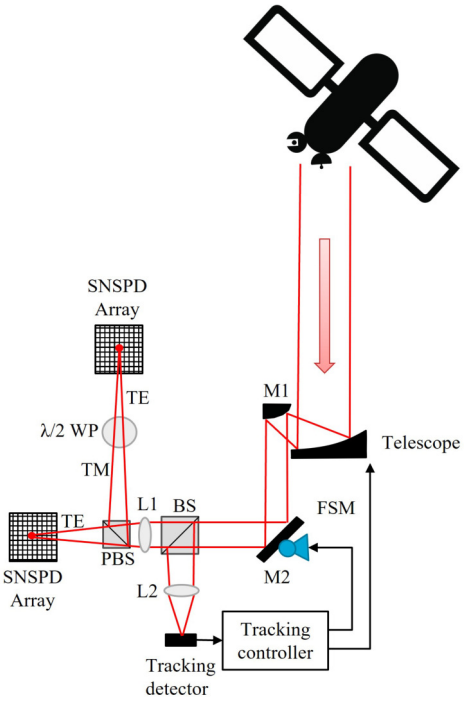

Figure 1. System view with .

We use a numerical optical propagation tool to estimate the spatiotemporal statistics in the focal plane of the receiving telescope, using the split step method to discretize the vertical profile. The angular spectrum method is used for the optical propagation between discretized vertical planes (phase screens). Once arrived in the telescope, the focal plane image is obtained by Fraunhofer propagation. We compare these statistics with a practical detector array implementation and its realistic spatial parameters. From this, we calculate the fractional power per detector pixel for weak turbulence ($D/r_0 = 2$) and strong turbulence ($D/r_0 = 8$).

2. SYSTEM DESCRIPTION

We consider a system, in which the source is located in the satellite. The satellite has a pointing mechanism, that directs the power of the beam towards a ground station. The optical beam traverses through the atmosphere to reach the optical ground station (OGS). The OGS has a telescope that focuses the beam on the detector.

2.1 Optical ground system

We consider two systems with slight differences, as shown in Fig. 1. Both systems consist of a telescope with a diameter of 1 m and an effective focal length of 6 m, mimicking a Plane Wave 1 m telescope.[7] An exception is that no central obscuration is taken into consideration, so the telescope is depicted as an off-axis parabola.

In order to correct for tip-tilt system (a) is depicted with a tip-tilt mirror. The tip-tilt or fast steering mirror can correct for tip-tilt aberrations that originate from the atmosphere and ground vibrations. Measuring the tip-tilt aberrations can be done by 2 means: i) focusing the beam on a tracking detector, which can be a quad cell, or an image detector (camera), and determining the center of gravity; ii) using a wavefront detector for measuring the tip-tilt in the phase. The measured tip-tilt aberrations are fed back using a feedback controller. It provides the control signal to a fast steering mirror (FSM) for fast aberrations, such as vibrations and atmospheric turbulences. Also it provides a control sign to the coarse pointing assembly (CPA) of the telescope, to compensates for slow aberrations, such as thermal drift. The total assembly makes sure that the light from the atmosphere is projected on the SNSPD.

2.2 Point spread function width

As the optical beam travels through turbulence, we need to consider two limit cases, the diffraction limit and the seeing limit. We consider these in the focal plane, to obtain a reasonable size of the detector array. The diffraction limit of the system with focal length $f = 6$m, diameter $D = 1m$, and the wavelength of $\lambda = 1550\,$nm, is 22 μm:

$$d_{spot} = 2.44\frac{\lambda f}{D}$$

The seeing limit through atmospheric turbulence is determined by the Fried parameter r_0. The seeing limit is expressed as[3]

$$d_{spot} = 2.44\frac{\lambda f}{r_0}$$

For a Fried parameter of 12.5 cm at 1550 nm, which is a representative number for urban environments, this is 180 μm, including tip-tilt aberrations. For a system that compensates for tip-tilt, the wavefront variance reduces from $(D/r_0)^{5/3}$ to $0.134(D/r_0)^{5/3}$,[8] indicating a reduction of a factor of 2.7.[9] So we expect an image size of about 65 μm.

2.3 SNSPD array description

The last element in the system is the SNSPD array. Superconducting nanowire single-photon detectors (SNSPD) are known for their combination of ultrahigh detection efficiencies, fast recovery, sub-10 picosecond time resolution, and broadband sensitivity window from X-ray to mid-infrared. These performance characteristics make SNSPDs an ideal choice for Laser satellite communications. SNPSD arrays have gained significant attention and have recently been tested for NASA's Deep Space Optical Communications project.[10] The NASA work has focused on specialized coatings to reduce polarization dependence of the SNSPD array. We adopt a different approach by splitting the incoming light into TE and TM polarizations, defined as being parallel and perpendicular to the SNSPD nanowires, respectively. A polarization beamsplitter is used for this purpose, and the two polarizations are detected independently in separate arrays. Assuming that the TE mode has a higher absorption, using a half waveplate, we convert the TM mode into TE mode. The converted light can then be detected either using a second array (as shown in the figure) or alternatively be folded back to the same array.

Taking into account the optical turbulence, when designing SNSPD arrays for satellite communications, several design and operation parameters must be carefully considered. In the following, we will review the design parameters for an SNSPD array.

2.3.1 SNSPD array size

Given the wavefront aberrations that will be discussed in detail in the following sections, a total active area of $100\times100\,\mu m^2$, for the SNSPD array, seems appropriate. To cover this relatively large area, an array of detectors is considered as it can deliver superior performance in terms of recovery time, time resolution, and yield, at the cost of more complexity. Smaller pixels enhance temporal performance (shorter recovery time and better time jitter) and yield (smaller pixels lead to smaller dead areas due to defects), but reduce overall efficiency and increase the costs and complexities. The reduction in efficiency is due to a decrease in the ratio of active sensor area to total area, which includes wiring and routing. Furthermore, because typical front-end sharing SNSPD readout techniques have limited detection rates, detectors used in optical communication generally require individual readout. The latter would impose an additional limitation on the total number of pixels. Here, we assume a 5×5 array that leads to $\sim 20 \times 20\mu m^2$ pixels. This arrangement will lead to a small wiring and routing overhead.

2.3.2 Coupling and detection efficiency

Including a safe pixel separation of $1\mu m$ for SNSPD's readout overhead, as discussed above, the detection efficiency of the array can be determined from that of a typical single-pixel detector which is easily calculated using the transfer matrix method for TE light (since here we convert TM light into TE, the same calculation holds for both polarizations).

2.3.3 Dark counts

There are two types of dark count associated with SNSPDs. The intrinsic dark counts, which usually appear at very high bias currents (close to the switching current), and extrinsic dark counts which are caused by stray light such as coupled blackbody radiation from elements in the optical path. For a detector with good internal efficiency (long plateau in efficiency vs current curve), the intrinsic dark counts can be minimized by under-biasing without any penalty on efficiency. When well isolated, SNSPDs can offer extremely low dark counts.[11,12] Light coupled from the telescope into SNSPDs must be stringently filtered at cryogenic temperatures to make sure blackbody radiated photons are removed as much as possible.

2.3.4 Temporal performance

The timing performance of the SNSPD arrays can be divided into recovery time and time jitter. Smaller detectors tend to have faster recovery times and lower time jitters. Sub-nano second recovery,[13] and sub-10 pico-second time jitter combined with high efficiency have been reported,[14] with a record time resolution of 2.5 ps for a short nanowire.[15] Our $20 \times 20 \mu m^2$ SNSPD pixels will have estimated recovery time of 50-70 ns. As pixels detect independently, after detecting a photon in a pixel, and while in recovery, other pixels can independently detect light, and hence the effective recovery time is shorter. A time jitter of about 20 ps is achievable with SNSPDs of these size.[16]

3. SIMULATION SETUP

3.1 Turbulence simulation overview

As the satellite is at least few 100 kilometers for low earth orbits (LEO)[17] to 40.000 km for geostationary satellites,[18] we assume the optical beam arrives as a plane wave on top of the atmosphere. The split step method is used, largely following the methodology described by Jason Schmidt.[19] The model consists of 8 layers at $[40.000, 20.000, 10.000, 5.8000, 2.500, 1.250, 600, 100]$ m. The phase screens at these layers of 2×2 m are generated with the Discrete Fourier Transform complemented with 9 subharmonics,[20] to obtain a sufficient amount of tip-tilt aberrations. Each phase screen consists of 256×256 pixels. The phase screens are windowed by a cosine windowing function of 32 pixels wide. To arrive from the last layer to the focal plane, a twofold zero-padding is used, to improve resolution in the focal plane, i.e. 512×512 pixels.

A modified Hufnagel-Valley (HV) is used, to arrive at a Fried parameter of 50 cm and 12.5 cm. The 12.5 cm Fried parameter is obtained using a HV57 model, with a zenith angle of 60 degrees, resulting in an isoplanatic angle of 9 μrad. The 50 cm is realized by multiplying this C_n^2 profile by 0.2. Although this is not based on thourough investigation of site properties, we do this to keep the ratio between the isoplanatic angle and the Fried parameter. The Fried parameter, the isoplanatic angle and the scintillation index are verified with analytic formulation,[4] which showed differences of maxumum 20%.

Using a Fried parameter of 50 and 12.5 cm in combination of a telescope diameter of 1 meter, this results in a D/r_0 of 2 and 8 respectively. These values of D/r_0 are chosen as a very mild and stronger condition.

For temporal evolution, we first validated that the PSF is not significantly changed due to higher altitude turbulence. This practically means that the shape of the PSF is dominated by the phase aberrations, and not by the amplitude aberrations in the pupil plane. With this finding, we create a long phase screen by stitching many phase screens together, using cross-fading. This long phase screen, is given a constant velocity of 21 m/s. The focal plane image is obtained by Fraunhofer propagation. Next, the irradiance of the focal plane $I(x, y, t)$ is used to obtain the power spectral density $PSD_I(x, y, f)$, with the temporal frequency f in Hz.

3.2 SNSPD simulation overview

As discussed above, we consider an array of 5×5 SNSPDs with $20 \times 20\,\mu m^2$ detector (pixel) sizes and $1\,\mu m$ separation between pixels. Transfer matrix calculations, neglecting the loss in telescope optics and transmission loss of cryostat window, yield a pixel absorption efficiency of about 98% with the following parameters: NbTiN film with a thickness of 10 nm, patterned into meandering pixels with fill factors of 50% (not to be confused with the fill factor of the array), and operated at the resonance of the cavity (7 layers of DBR, SiO_2/Nb_2O_5, optimized for the wavelength of 1550 nm). Now overlaying this information on the intensity patterns leads to the

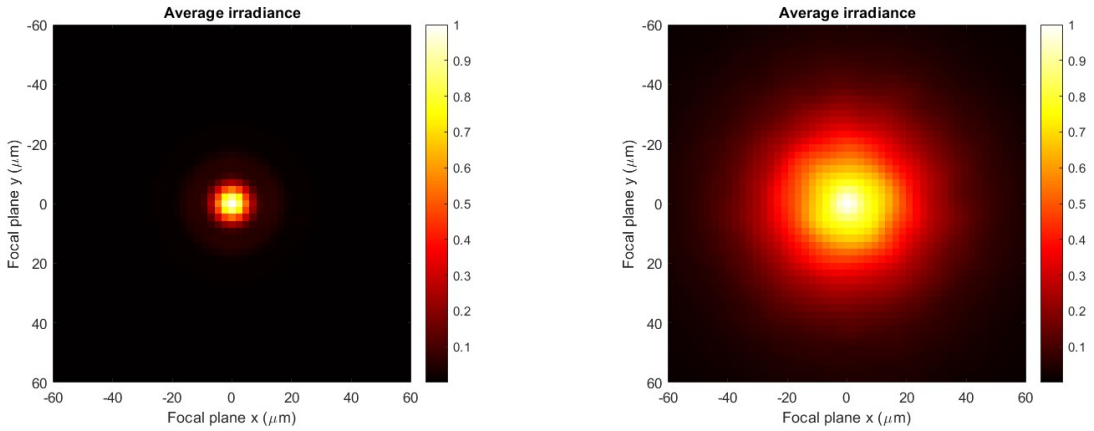

(a) (b)

Figure 2. Average irradiance over 4000 samples: (a) $D/r_0 = 2$, (b) $D/r_0 = 8$.

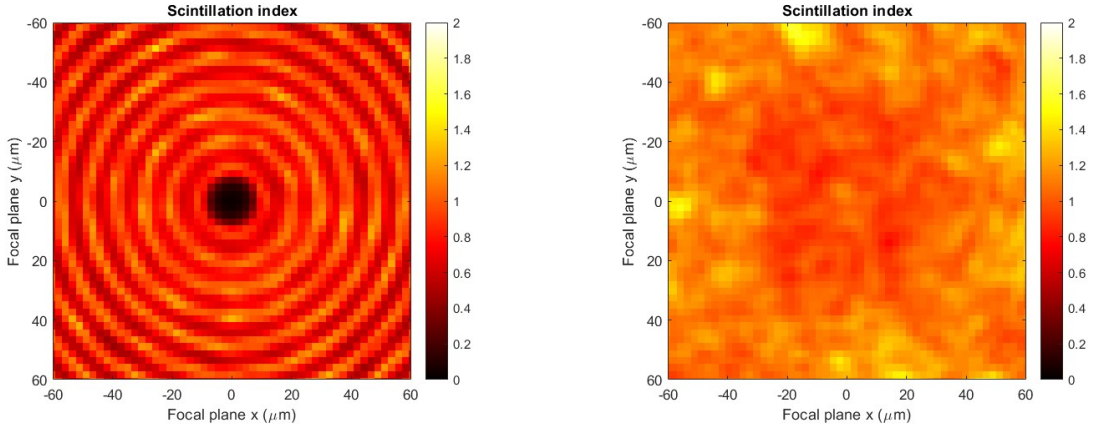

(a) (b)

Figure 3. Scintillation index over 1000 samples: (a) $D/r_0 = 2$, (b) $D/r_0 = 8$.

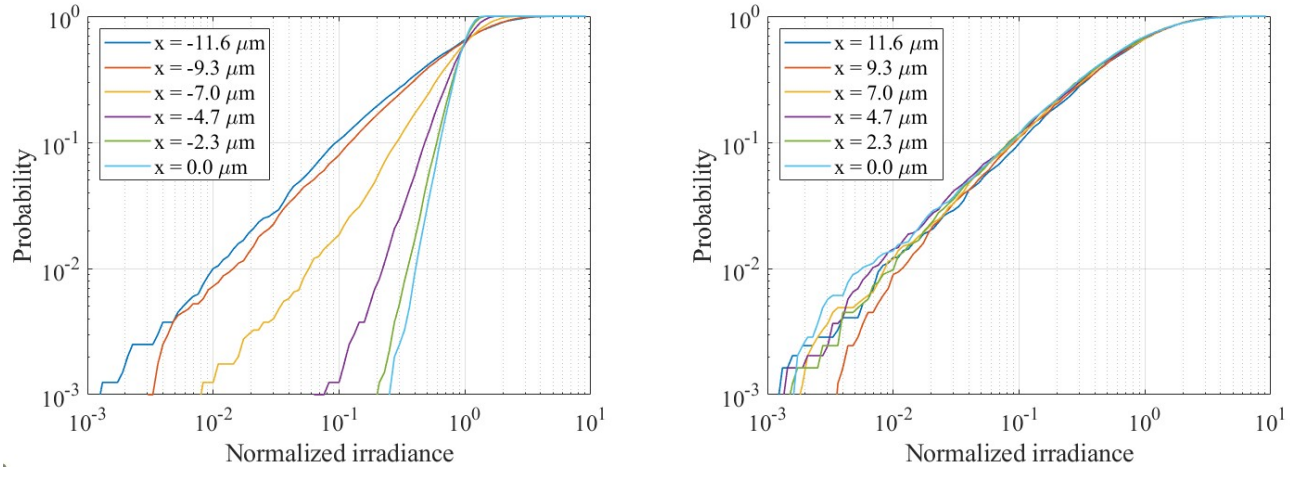

(a) (b)

Figure 4. Cumulative density functions (CDF) of (a) $D/r_0 = 8$ and $D/r_0 = 2$. Tip, tilt correction is on.

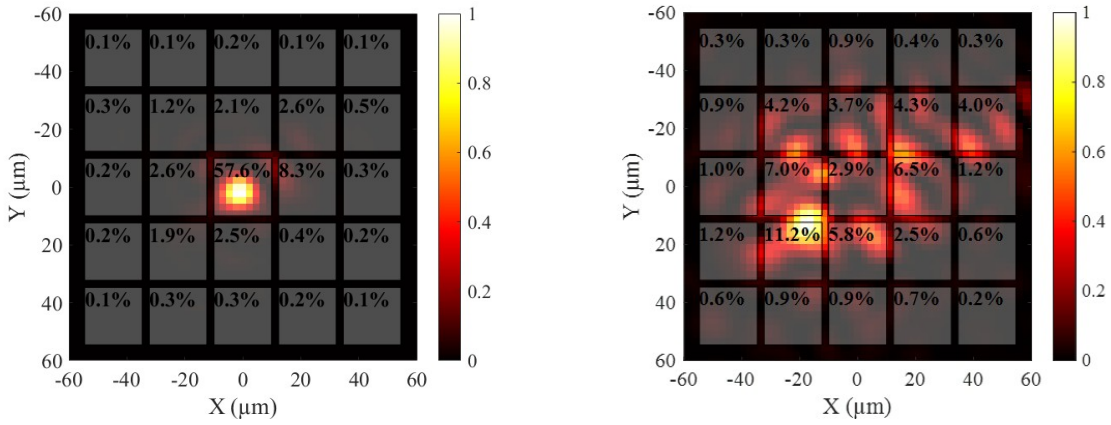

(a) (b)

Figure 5. One sample of a detector map, with relative irradiance: (a) $D/r_0 = 2$, (b) $D/r_0 = 8$.

data shown in Figures 5a and Figures 5b. It is clear that without turbulence, the central pixel gets most of the intensity, and hence may be overwhelmed or under-perform. For such a case, an optical diffuser, or alternatively, an interleaved design of SNSPD array may be necessary. However, the former may produce extra losses and the latter, although doable,[10] increases the complexity (in terms of fabrication and avoiding thermal and RF crosstalk). In the presence of turbulance, as shown in Figure 5b, this is not a major problem.

4. RESULTS

4.1 Average intensiy/spot size

Average irridiance profiles in the focal plane of the telescope are depicted in Figure 2. As expected, the diameter of weak turbulence ($D/r_0 = 2$) is close to the diffraction limit. For strong turbulence ($D/r_0 = 8$), the spot size increased considerably. As can be seen from the plot, the estimate of 65 μm was quite accurate.

4.2 Scintillation index

Over 4000 samples, we have estimated the scintillation index as a function over space by:

$$\sigma_I^2(x,y) = \frac{\langle I^2(x,y)\rangle - \langle I(x,y)\rangle^2}{\langle I(x,y)\rangle^2} \tag{1}$$

$\sigma_I^2(x,y)$ = The result of this is shown in Figure 3. For weak turbulence, ($D/r_0 = 2$), the scintillation index is low within the spot of the beam. Beyond the spot, the scintillation index increases. This is to be expected, as the intensity is quite high in the center of beam, and it is kept at its position using the FSM. Outside of the spot, the irradiance might fluctuate slightly, as the turbulence mainly effects the Airy rings for low turbulence. What is also observed is the location of those Airy rings. The reason why this happens is evident using similar reasoning, i.e. the scintillation index is the highest at the nominal position of the dark rings. For strong turblence ($D/r_0 = 8$), the scintillation index gets into the saturated regime. Also this is easy to explain. The spot breaks up in the focal plane. The location of those spots on the detector is random, so dark and bright spots are fluctuating over time, from completely dark to completely bright.

4.3 Probability density functions

From the obtained irradiance profiles, the cumulative probabilities are obtained, as this is assumed to be informative on e.g. estimating the bit error rate for classical communications. The CDF is probed per pixel, in the radial direction from the center of the spot, to see any variation in this direction. For strong turbulence ($D/r_0 = 8$), the distribution of the CDF is relatively homogeneous. Considering the uniformity of the scintillation index, this comes as no surprise. More variation could be expected in the weak turbulence case ($D/r_0 = 2$), which is indeed the case. In the center of the spot, the CDF is very steep, at a value of 0.2 at a BER of 10^{-3}. Going radially outward, the CDF is going towards the same values as for the strong turbulence case.

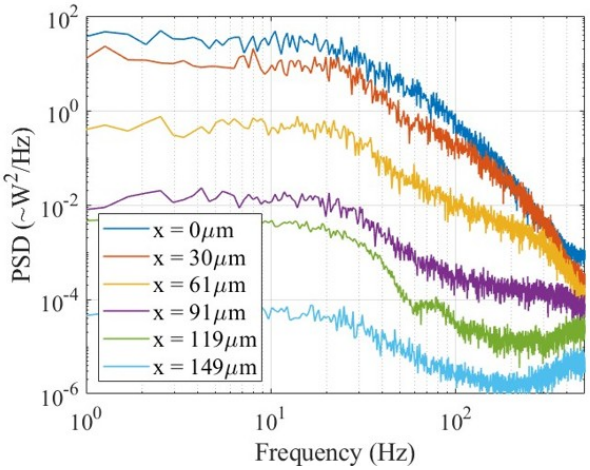

Figure 6. Power spectral density (PSD) when $D/r_0 = 8$. PSD is with different distances from the center. Tip-tilt correction is off.

4.4 SNSPD detector performance

The projection of the spots on the pixelated detector is shown in Figure 5. In the used model for the detector, no advanced physics mechansisms are (currently) used. The only losses accounted for are the light that drops into the bandguard, which is one pixel, equating 2.33 µm and the SNSPD efficiency of 98%. The total accumulated power in strong turbulence conditions is 64%. Main reason for this value is that some bright spots are sitting on top of the bandguards. As the value for the bandguard, is relatively high in our simulation, it is expected that this is a conservative estimate. For weak turbulence, the total accumulated percentage is 82%. Also here, quite some light is projected in the bandguard, causing a significant loss. The peak intensity is 58% for weak compared to 11% for strong turbulence.

4.5 Power spectral density

The power spectral density (PSD) in the focal plane, is shown of several radial positions in the focal plane, see Figure 6. What is interesting, is that the cut-off frequency is at the same frequency for all detector positions. The cut-off frequency is proportional to the wind speed v_{wind} and inversely proportional to the diameter of the telescope, so yielding a value of around 20 Hz. The reason is that the telescope provides an averaging effect. The v_{wind}/D ratio is the refresh ratio of the phase aberations.

4.6 Overall systems performance

First, we compare the recovery time of the detector and the time constant of the intensity fluctuations. Because the recovery time of the detector of 100s of picoseconds is of a totally different order of magnitude of the turbulence fluctuations of 100s of ms, those time scales are not expected to influence each other. So, the detection cannot benefit from the temporal aspects of the turbulence fluctuations. What it can benefit from, is the wider spread of the point spread function, i.e. the flux is per pixel is lower at a persistent integrated power level. In this paper we only do a direct comparison based upon the images Figure 6. As the maximum flux with strong turbulence is 11% and 58% for weak turbulence. Hence, the turbulence is improving the illumination uniformity on the detector, which increases the efficiency of the detection.

4.7 Conclusions

In this paper, we investigated the focal plane statistics, with the goal to estimate the efficacy of SNSPDs. We presented an optical system, without the use of complicated adaptive optics. The beam travels from the satellite through the atmosphere towards the ground station. The turbulence strengths we investigated have a Fried parameter of 50 and 12.5 cm respectively, representing a D/r_0 of 2 and 8. The width of the long term averaged point spread function is 4× larger for this case. The scintillation index is hardly a function of the position in

the focal plane, as long as the spot is sufficiently covering its position. Hence, also the PDF is similar over the focal plane, except for the weak turbulence case, which is very steep in the center of the spot, and progresses towards the PDF of the strong turbulence case, for an off-axis point. The temporal characteristics, are mainly varying due to ratio of wind speed and diameter aperture. This with a 100 ms order of magnitude, which is signficantly larger compared to the recovery time of an SNSPD. Hence, the improvement that could be made is due to decreased flux per pixel, for more stronger turbulence conditions. While the results are interesting, we would like to emphasize the need for more thorough investigations which also include the photon flux dependence of SNSPD efficiency.

4.8 Acknowledgement

I. E. Z. acknowledges funding from the European Union's Horizon Europe research and innovation programme under grant agreement No. 101098717 (RESPITE project) and No.101099291 (fastMOT project).

REFERENCES

[1] Hemmati, H., [*Near-Earth Laser Communications*], CRC Press (2009).

[2] Bennett, C. H. and Brassard, G., "An update on quantum cryptography," in [*Workshop on the theory and application of cryptographic techniques*], 475–480, Springer (1984).

[3] Hardy, J., [*Adaptive Optics for Astronomical Telescopes*], Oxford University Press, New York (1998).

[4] Andrews, L. and Phillips, R., [*Laser beam propagation through random media*], SPIE press (2005).

[5] Charnotskii, M., "Statistical modeling of the point spread function for imaging through turbulence," *Optical Engineering* **51**, 101706 (2012).

[6] Engineering, D. T. O. and 2011, u., "Reanalysis of turbulence effects on short-exposure passive imaging," *spiedigitallibrary.org* .

[7] Plane Wave Instruments, "CDK 1000, https://planewave.com/products/cdk1000/."

[8] Noll, R. J., "Zernike polynomials and atmospheric turbulence," *Journal of the Optical Society of America* **66**, 207 (3 1976).

[9] Fried, D. L., "Optical Resolution Through a Randomly Inhomogeneous Medium for Very Long and Very Short Exposures KXR ?," *JOSA* **56**(10), 1372–1379 (1966).

[10] Wollman, E. E., Allmaras, J. P., Beyer, A. D., Korzh, B., Runyan, M. C., Narváez, L., Farr, W. H., Marsili, F., Briggs, R. M., Miles, G. J., and Shaw, M. D., "Snspd-based detector system for nasa's deep space optical communications project," *Opt. Express* **32**, 48185–48198 (Dec 2024).

[11] Shibata, H., Shimizu, K., Takesue, H., and Tokura, Y., "Ultimate low system dark-count rate for superconducting nanowire single-photon detector," *Opt. Lett.* **40**, 3428–3431 (Jul 2015).

[12] Hochberg, Y., Charaev, I., Nam, S.-W., Verma, V., Colangelo, M., and Berggren, K. K., "Detecting sub-gev dark matter with superconducting nanowires," *Phys. Rev. Lett.* **123**, 151802 (Oct 2019).

[13] Münzberg, J., Vetter, A., Beutel, F., Hartmann, W., Ferrari, S., Pernice, W. H. P., and Rockstuhl, C., "Superconducting nanowire single-photon detector implemented in a 2d photonic crystal cavity," *Optica* **5**, 658–665 (May 2018).

[14] Esmaeil Zadeh, I., Los, J. W. N., Gourgues, R. B. M., Chang, J., Elshaari, A. W., Zichi, J. R., van Staaden, Y. J., Swens, J. P. E., Kalhor, N., Guardiani, A., Meng, Y., Zou, K., Dobrovolskiy, S., Fognini, A. W., Schaart, D. R., Dalacu, D., Poole, P. J., Reimer, M. E., Hu, X., Pereira, S. F., Zwiller, V., and Dorenbos, S. N., "Efficient single-photon detection with 7.7 ps time resolution for photon-correlation measurements," *ACS Photonics* **7**(7), 1780–1787 (2020).

[15] Korzh, B., Zhao, Q.-Y., Allmaras, J. P., Frasca, S., Autry, T. M., Bersin, E. A., Beyer, A. D., Briggs, R. M., Bumble, B., Colangelo, M., Crouch, G. M., Dane, A. E., Gerrits, T., Lita, A. E., Marsili, F., Moody, G., Peña, C., Ramirez, E., Rezac, J. D., Sinclair, N., Stevens, M. J., Velasco, A. E., Verma, V. B., Wollman, E. E., Xie, S., Zhu, D., Hale, P. D., Spiropulu, M., Silverman, K. L., Mirin, R. P., Nam, S. W., Kozorezov, A. G., Shaw, M. D., and Berggren, K. K., "Demonstration of sub-3 ps temporal resolution with a superconducting nanowire single-photon detector," *Nature Photonics* **14**, 250–255 (Apr 2020).

[16] Chang, J., Zadeh, I. E., Los, J. W. N., Zichi, J., Fognini, A., Gevers, M., Dorenbos, S., Pereira, S. F., Urbach, P., and Zwiller, V., "Multimode-fiber-coupled superconducting nanowire single-photon detectors with high detection efficiency and time resolution," *Appl. Opt.* **58**, 9803–9807 (Dec 2019).

[17] Klop, W., Saathof, R., Doelman, N., Gruber, M., Moens, T., Klop, A. W., Osorio Tamayo, C. I., and Duque, C., "QKD optical ground terminal developments," *International Conference on Space Optics* **11852**, 388–403 (6 2021).

[18] Dirks, B. P. F., Ferrario, I., Le Pera, A., Finocchiaro, D. V., Desmons, M., De Lange, D., De Man, H., Meskers, J. H., Morits, J., Neumann, N. M. P., Saathof, R., and Witvoet, G., "GEOQKD: quantum key distribution from a geostationary satellite," *spiedigitallibrary.org* **11852**, 118520–118521.

[19] Schmidt, J. D., [*Numerical simulation of optical wave propagation with examples in MATLAB*] (2010).

[20] Charnotskii, M., "Comparison of four techniques for turbulent phase screens simulation," *Journal of the Optical Society of America A* **37**, 738 (5 2020).